Reaction Kinetics, Mechanisms and Catalysis
https://doi.org/10.1007/s11144-022-02272-0

Tuning the reactivity of ruthenium(II) terpyridyl complexes using auxiliary ligands: kinetic and mechanistic studies

Gershom Kyalo Mutua[1,2] · **Meshack Sitati**[1,3] · **Daniel O. Onunga**[1,4] · **Deogratius Jaganyi**[5,6] · **Allen Mambanda**[1]

Received: 1 June 2022 / Accepted: 21 July 2022

Abstract

Substitution behavior of the labile aqua ligand in four mononuclear ruthenium(II) terpyridyl complexes with different auxiliary N (pyridine) (**Ru1**), N^N (2,2′-bipyridyl (**Ru2**), 2′-(2-pyridyl)quinoline (**Ru3**), 2,2′-biqunoline (**Ru4**) ligands was investigated using three nucleophiles; thiourea, 1,1-dimethylthiourea and 1,1,3,3-tetramethylthiourea. The effect of concentration and temperature on the substitution behavior of the complexes were studied under *pseudo*-first order conditions using UV–Vis spectrophotometer. The second order rate constants (k_2) of the aqua complexes decreased in the order: **Ru4** > **Ru3** > **Ru1** > **Ru2**. The results showed that the rate of substitution of the aqua ligand increased with an increase in the π-surface area of the N^N bidentate auxiliary ligands. This is attributable to an upsurge in π-back-donation and electrophilicity of the complexes as the π-extension of the auxiliary ligands increases. **Ru2** is less reactive than **Ru1** due to the increased steric hinderance introduced by the 2,2′-bipyridyl bidentate auxiliary ligand in **Ru2** compared to **Ru1** which has two independent *trans* pyridines. From computational results, it was observed that as the aromatic surface area of the auxiliary ligand increased from **Ru1**–**Ru4**, the HOMO–LUMO gap decreased accordingly. Consequently, the chemical softness and electrophilicity of the complexes increased accordingly. This is corroborated by the decrease in pKa values of the complexes as one moves from **Ru1** to **Ru4**. As a result, the nucleophilic attack becomes facile from **Ru1** to **Ru4**. All the reactions follow an associative interchange mechanism as indicated by the positive activation enthalpy and negative activation entropy. The crystal structure of bipyridylterpyridylthiourearuthenium(II) perchlorate show that the substitution product obtained is stable.

Keywords Substitution · Ruthenium(II) · Kinetics · Auxilliary ligands · Nucleophiles

✉ Gershom Kyalo Mutua
gmutua@mmust.ac.ke

Extended author information available on the last page of the article

Published online: 28 July 2022

Introduction

Ruthenium complexes are suitable for many applications because of their well-established coordination chemistry and their existence in several oxidation states [1, 2]. Terpyridine-based complexes form a key class of polypyridyl ruthenium complexes with uses spread over different areas such as medicine and catalysis [3–5]. The role played by substituents attached to the terpyridine backbone on the substitution behavior of leaving ligands in metal complexes is well documented. These studies have established that electron-withdrawing substituents make the complexes more electrophilic hence enhancing the substitution of the labile ligand, while electron-donating groups can enhance or reduce the reactivity of a complex [6, 7]. The extension of π-conjugation of the terpyridine framework affects substitution reactivity of metal complexes in two different ways, depending on the position and location at which the changes occur on the ligand. For example; replacing the pyridine moieties with quinoline at the lateral positions retards the displacement of the labile ligands by destabilizing the lowest unoccupied molecular orbital [7, 8].

Studies have also reported that auxiliary ligands on terpyridine ruthenium(II) complexes confer both steric and electronic effects depending on their nature. For example, it was observed that when ethylene diamine bidentate auxiliary ligand was replaced by 2,2′-bipyridyl auxiliary ligand, the rate of substitution of the aqua labile ligand reduced 60 times. This is so despite bipyridyl ligand being a better a better π acceptor compared to ethylene diamine. The drastic dampening of the reactivity is attributable to increased steric hinderance to the incoming group by the 2,2′-bipyridyl bidentate auxiliary ligand [9]. This is further reinforced by a study by Milutinović and co–co-workers in which, when aliphatic auxiliary bidentate ligands was replaced by 2,2′-bipyridyl the substitution reactivity drastically reduced [10]. Like-wise for aquation reactions replacement of 2,2′-bipyridyl auxiliary ligand by phenathroline, reduced the reaction rate significantly. This is attributed to increased steric hinderance of the latter compared to the former, thus impeding access to the metal centre [9, 11]. On the other hand, when 1,10-phenathroline is replaced by 2,9-dimethyl-1,10-phenathroline, the rate of reactivity was observed to increased by *ca*. 600 folds. This can be explained by the fact that the methyl substituents on the auxiliary ligand donates electron density to the metal centre, thus enhancing the rate of substitution of the labile ligand [12, 13]. Contrarily, there is no much information on the substitution behavior of the labile group in terpyridyl ruthenium(II) when π-surface area of the auxiliary ligands is systematically varied.

Given the wide applications of terpyridine based complexes, terpyridine was used as the anchor ligand in the meridional plane of these octahedral complexes. This was done to establish the role of extending the π-conjugation of the facially *N*,*N*-coordinated auxiliary ligand (N^N) on the lability of the aqua leaving group. The study was carried out using biologically important thiourea nucleophiles; thiourea, 1,1-dimethylthiourea and 1,1,3,3-tetramethylthiourea. These nucleophiles have high nucleophilicity and solubility [14]. The auxiliary ligands (N/N^N) used were; pyridine (**Ru1**), 2,2′-bipyridine (**Ru2**), 2-(2-pyridyl)quinoline (**Ru3**) and 2,2′-bisquinoline (**Ru4**). Fig. 1 shows the molecular strucutures of complexes studied.

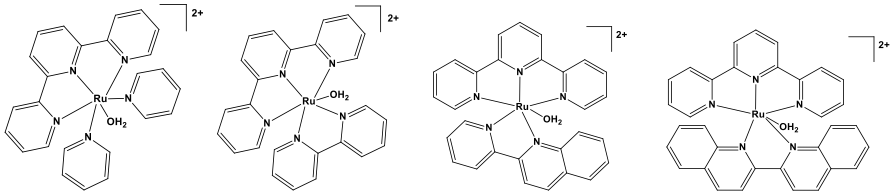

Fig. 1 Molecular structures of the studied ruthenium(II) aqua complexes

To establish the theoretical trends in the ground-state structural and electronic data of the complexes, their energy- and geometry-optimized structures were computed by density functional theory. The retrieved data were used to corroborate experimentally observed substitution reactivity trends of the complexes.

Experimental section

Materials and methods

All the syntheses were performed under an inert dinitrogen atmosphere. 2,2′:6′,2′-terpyridine (terpyridine) (98%), 2, 2′-bipyridyl (99%), anhydrous pyridine (≥ 99%), $RuCl_3{\cdot}3H_2O$, $NaBF_4$ (98%), $HClO_4$ (70 wt% solution), NH_4PF_6 (≥ 99%), 2,2′-biquinoline (98%), LiCl (≥ 99%), triphenylphosphine (99%), NaOH (≥ 97%), HCl (37%), triethylamine (≥ 99.5%), $AgClO_4$ (99%), $NaClO_4{\cdot}H_2O$ (98%), Thiourea (≥ 99%), 1,1-dimethylthiourea (99%) and 1,1,3,3-tetramethylthiourea (98%) were bought from Merck (Pty). 2-(2-pyridyl)quinoline was synthesized as per established method [15] (ESI 1). All the organic solvents used in this study were supplied by Merck (Pty).

Syntheses of the chloro ruthenium(II) complexes

The chloro ruthenium(II) complexes were synthesized as per reported established literature methods [12, 16–19].

Trichloro(terpyridyl)ruthenium(III)

In 90 mL of ethanol, a mixture of terpyridine (349.5 mg, 1.5 mmol) and $RuCl_3{\cdot}3H_2O$ (393.0 mg, 1.5 mmol) was refluxed for 4 h with a continuous agitation. The reaction mixture was then cooled to ambient temperatures and the brown solid that formed was filtered off and washed thrice with 30 mL of absolute ethanol and thrice with 30 mL of diethyl ether. The precipitate was dried in vacuum to obtain a powder. Yield: 569 mg, 86%. This complex was used in the syntheses of all the ruthenium(II) chloro complexes.

***Trans*-chloro*bis*(pyridyl)(terpyridyl)ruthenium(II) hexaflourophosphate**

Triphenylphosphine (472.0 mg, 18 mmol), trichloro(terpyridyl)ruthenium(III) (200.0 mg, 0.45 mmol), and triethylamine (1 mL) were mixed in chloroform (45 mL) and refluxed for 3 h until the reaction mixture turned violet in colour. Absolute ethanol (30 mL) was added to the cooled violet solution and the mixture was subsequently concentrated to *ca*. 10 mL, yielding a violet precipitate. The precipitate was filtered off and re-dissolved in a minimum volume of a mixture of warm chloroform and absolute ethanol (1:1). The addition of diethyl ether precipitated a dark violet coloured solid. The obtained solid was dissolved in anhydrous pyridine (50 mL) and refluxed for additional 2 h. The solution was then evaporated to dryness and the residue re-dissolved in deionized water (30 mL). The complex was precipitated off by addition of saturated aqueous NH_4PF_6 solution. The complex obtained was filtered off and washed with a copious amount of diethyl ether and dried under reduced pressure. Yield: 168.0 mg (56%). ESI^+-TOF MS (m/z): 528.00 (M^+). Elemental Analysis: Calculated for $C_{25}H_{21}ClN_5PF_6Ru$; C, 44.62; H, 3.15; N, 10.41. Found: C, 44.38; H, 3.21; N, 10.28. ^1H NMR (400 MHz, DMSO-d_6, ppm): δ = 9.19 (d, 2H), 8.66 (m, 4H), 8.15 (t, 2H), 8.01 (t, 1H), 7.93 (d, 4H), 7.86 (t, 2H), 7.60 (t, 2H), 7.09 (t, 4H). ^{13}C NMR (400 MHz, DMSO-d_6, ppm): δ = 160.9, 158.9, 152.7, 152.2, 137.9, 137.4, 132.5, 129.2, 125.1, 124.7, 124.1.

(2,2′-Bipyridyl)chloro(terpyridyl)ruthenium(II) chloride

A mixture of 2,2-bipyridine (142.0 mg, 0.91 mmol), trichloro(terpyridyl) ruthenium(III) (400.0 mg, 0.91 mmol), trimethylamine (1 mL) and LiCl (212.0 mg, 5 mmol) in 40 mL of absolute ethanol–water (3:1) solvent mixture was refluxed for 4 h. The hot solution obtained was filtered and concentrated to *ca*. 10 mL. The concentrated solution was chilled at 4 °C for 48 h and the solids that formed were filtered off and washed with 20 mL of 3 M HCl, 30 mL of acetone and excess amount of diethyl ether. The solids were then dried under reduced pressure. Yield: 352.1 mg (69%). ESI^+-TOF MS (m/z): 526.04 (M^+). Elemental Analysis: Calculated for $C_{25}H_{19}Cl_2N_5Ru.2H_2O$; C, 50.26; H, 3.88; N, 11.72. Found: C, 49.91; H, 3.97; N, 11.64. ^1H NMR (400 MHz, DMSO-d_6, ppm): δ = 10.11 (d, 1H), 8.94 (d, 1H), 8.84 (d, 2H), 8.71 (d, 2H), 8.66 (d, 1H), 8.38 (t, 1H), 8.24 (t, 1H), 8.08 (t, 1H), 8.00 (t, 2H), 7.79 (t, 1H), 7.63 (d, 2H), 7.40 (t, 2H),7.33 (d, 1H), 7.10 (t, 1H). ^{13}C NMR (400 MHz, DMSO-d_6, ppm): δ = 158.9, 158.1, 156.2, 152.4, 151.9, 151.5, 136.9, 136.6,134.1, 127.1, 126.7, 126.1, 123.4, 123.2, 122.3

***Proximal*-Chloro(2-(2-pyridinyl)quinoline)(terpyridyl)ruthenium(II) chloride**

A mixture containing 2-(2-pyridinyl)quinoline (93.0 mg, 0.45 mmol), trichloro(terpyridyl)ruthenium(III) (200.0 mg, 0.45 mmol), trimethylamine (0.1 mL) and LiCl (19.0 mg, 0.45 mmol) in absolute ethanol–water (3:1) solvent system (40 mL) was refluxed for 5 h. The obtained purple solution was filtered while still hot and concentrated to *ca*. 5 mL. The concentrated solution was then cooled to room temperature and refrigerated at 4 °C for 48 h. The purple filtrate that formed

was filtered off and was washed with 0.1 mL of 3 M HCl, 2.5 mL of acetone and 10 mL of diethyl ether. Yield: 230.2 mg (71%). ESI^+-TOF MS (m/z): 576.5 (M^+). Elemental Analysis: Calculated for $C_{29}H_{21}ClN_5PF_6Ru.H_2O$; C, 47.13; H, 3.14; N, 9.48. Found: C, 47.02; H, 3.45; N, 9.37. ^{1}H NMR (500 MHz, CD_3OD-d_4, ppm): δ = 10.65 (d, 1H), 9.03 (d, 1H), 8.93–8.85 (m, 4H), 8.75 (d, 2H), 8.36 (d, 1H), 8.29 (t, 1H), 8.04 (t, 2H), 7.94–7.87 (m, 5H), 7.76 (d, 1H), 7.38 (t, 2H), 7.23 (t, 1H). ^{13}C NMR (500 MHz, CH_3OD-d_4, ppm): δ = 160.2, 159.0, 158.9, 157.2, 152.9, 151.6, 151.0, 138.3, 137.3, 135.2, 131.0, 129.8, 129.0, 128.4, 127.2, 125.9, 125.0, 123.7, 122.6, 118.9.

(2,2′-Biquinoline)chloro(terpyridyl)ruthenium(II) hexafluorophosphate

In 50 mL of absolute ethanol–water (3:1) solvent system, a mixture of trichloro(terpyridyl)ruthenium(III) (200.0 mg, 0.45 mmol) 2,2′-biquinoline (115.3 mg, 0.45 mmol), trimethylamine (0.1 mL) and LiCl (20.0 mg, 0.47 mmol) was refluxed for 5 h. The hot solution obtained was filtered to remove unreacted materials. Then 5 mL of saturated solution of NH_4PF_6 was added to the filtrate and the resulting solution chilled at 4 °C for a day. The cold solution was filtered and concentrated to *ca*. 10 mL. The solids that appeared were filtered off and re-dissolved in dichloromethane-methanol (9:1) solvent system. The solution was then flushed through a column packed with alumina, where the initial purple-blue band was collected. The extract was added an equal volume of toluene and concentrated to *ca*. 6 mL. The crystalline solids that appeared was filtered off, washed with 10 mL of toluene and excess amount of diethyl ether. The solid was then dried under reduced pressure. Yield: 197.9 mg (58%). ESI^+-TOF MS (m/z): 626.06 (M^+). Elemental Analysis: Calculated for $C_{33}H_{23}ClN_5PF_6Ru$; C, 51.40; H, 3.01; N, 9.08. Found: C, 51.78; H, 3.21; N, 8.95. ^{1}H NMR (400 MHz, CD_3OD-d_4, ppm): δ = 9.90 (d, 1H), 9.11 (d, 1H), 9.01 (d, 1H), 8.82(d, 1H), 8.76 (d, 2H), 8.60 (d, 2H), 8.37 (d, 2H), 8.28 (t, 1H), 8.02–7.84 (m, 8H), 7.53 (t, 1H), 7.42 (t, 2H), 6.94 (d, 1H). ^{13}C (100 MHz, CD_3OD-d_4, ppm): δ (ppm) = 161.8, 159.3, 159.0, 156.1, 152.5, 151.8, 151.1, 138.3, 137.4, 136.9, 136.3, 135.4, 130.7, 130.3, 129.6, 129.0, 128.5, 128.3, 127.5, 127.0, 123.5, 122.5, 120.2, 119.1.

Physical measurements and instrumentation

^{1}H and ^{13}C NMR spectra of the complexes were obtained using Bruker Avance DPX III 400 or 500 MHz spectrometer with all the chemical shifts expressed in ppm and referenced to $Si(CH_3)_4$. Mass spectra were recorded using an ESI^+ TOF Micromass LCT Premier spectrometer. MS, ^{1}H and ^{13}C spectra the chloro complexes are presented in the Electronic Supplementary Information (Figs. S3–S17). Thermo Scientific Flash 2000 analyzer was used for the elemental analyses of carbon, hydrogen, and nitrogen in the complexes. pH titration studies and substitution studies were monitored using Cary Bio UV–Vis spectrophotometer with a temperature control unit (± 0.05 °C). Jenway 4330 combined pH and conductivity

meter was used to measure the pH of the aqueous solutions. Analysis of pKa titration and kinetics data was performed using OriginPro 9.1® program [20].

Conversion of the chloro complexes to aqua complexes

The chloro complexes were aquated to their corresponding aqua complexes by reacting equimolar amounts of the chloro complexes and $AgClO_4$ in 0.01 M $HClO_4$ solution in dark at 45 °C for 2 days. After cooling the solutions to room temperature, the AgCl precipitate wa filtered off using a 0.2 µM Millipore nitrocellulose membrane. The filtrate was diluted to an appropriate volume to obtain stock solutions (*ca*. 1 mM) of the ruthenium(II) aqua complexes [21]. Working solution for pKa titrations and substitution studies were obtained by diluting the stock solution.

Determination of acidity constants of the aqua complexes

The acidity constants of the ruthenium(II) aqua complexes were determined at 25 °C by titrating the complexes with NaOH. In each experiment, 500 mL of the complexes was used to minimize dilution effects [22]. Between pH 2 and 3, small portions of powdered NaOH were added using a micro-spatula to the solution of the ruthenium(II) aqua complexes while for pH above 3, drops of very dilute NaOH solutions of varying concentrations were used. After every addition of the base, the solution mixture was stirred for 2 min before measuring the pH and determining the corresponding UV–Vis spectrum. Aliquots used for the pH measurement were discarded while those used for the UV–Vis absorbance determination were returned to the titration solution.

Kinetic measurements

The concentration of the aqua complexes used in this study were; 0.42 mM (**Ru1**), 0.16 mM (**Ru2**), 0.48 mM (**Ru3**), 0.31 mM (**Ru4**). In all the experiments, the solutions of aqua complexes and nucleophiles were kept at pH = 1.0 and ionic strength = 0.1 M $HClO_4/NaClO_4$. The kinetic studies were carried out under *pseudo*-first order conditions; the concentration of the nucleophiles were at minimum 10 times higher than that of the metal complexes. The changes in UV–Vis absorbance arising from the reactions were monitored from 900 to 200 nm. The effects of nucleophilic concentration was monitored at 25 °C at varying nucleophilic concentration. The effect of temperature on substitution reactivity was investigated at constant concentration of nucleophiles but at different temperatures (25, 30, 35, 40 and 45 °C). All the reactions were commenced by mixing equivolumes of thermostated complex and nucleophile solutions in a divided cuvette. The presented rate constants are averages of atleast three runs.

Density functional theoretical studies

Calculations were executed by the Gaussian 09 W group of programs [23].The geometry-optimized structures of the Ru(II) aqua complexes were obtained at the density functional level of theory (DFT) using Becke's 3-hybrid parameters of the Lee–Yang–Parr method incorporating the standard LANL2DZ basis set [24]. DFT uses electron density over a set of wave functions for calculating the energy-minimized and geometry-optimized structure of a compound. Its structural data is accurate for most transitional metal complexes like the ones studied herein, which have a large number of electrons on the central Ru^{2+} ion [25]. To account for the inner 28 electrons of Ru^{2+} ion, the LANL2DZ basis set uses effective core potentials (ECP) [26]. The complexes were optimized in aqueus media using the CPCM implicit solvent model [27]. The complexes were optimized in their singlet spin ground states and dicationic (+2) point charges. Quantum chemical descriptors such as; chemical hardness, dipole moment, chemical softness, electronic chemical potential, and electrophilicity indices for the optimized aqua complexes were determined using reported methods [28–31]. Natural bond orbitals (NBO) analysis was employed to calculate atomic charges in the studied complexes.

Crystallographic analysis of substitution product

Crystals of bipyridineterpyridinethiourearuthenium(II) perchlorate were obtained by reacting aqueous **Ru2** (in aqueous 0.1 M $HClO_4/NaClO_4$) with excess thiourea at ambient temperatures. The resultant solution was then allowed to crystallize by slow evaporation of the solvent. A suitable crystal of this compound was then selected and mounted onto the Bruker Smart Apex II CCD diffractometer equipped with Oxford Instruments Cryojet nitrogen jet. The crystal was illuminated with a monochromatic MoKα1 ($\lambda = 0.71073$ Å) radiation and the resulting diffraction intensities recorded using the ω-2θ scan mode at a range of $1.896 < \theta < 27.450°$. The crystal structure was solved by Olex2-supported Shelxs program using direct methods and refined by full matrix least squares on F^2 on all the observed reflections [32, 33].

Results

pKas of the aqua complexes

The acidity constants of the aqua ligand in the all the complexes were determined by fitting a sigmoidal function (Eq. 1) onto the plot of absorbance (at a specific wavelength) versus pH.

$$y = A_2 + (A_1 - A_2)/(1 + \exp((x - x_0)/dx) \quad (1)$$

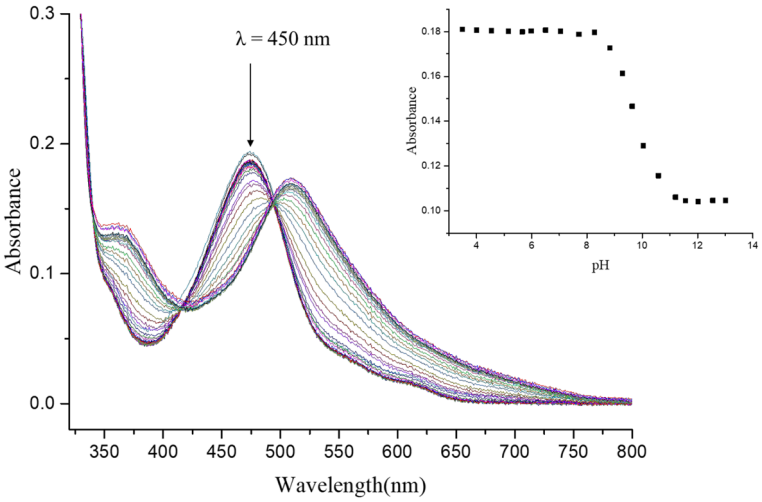

Fig. 2 UV–Vis spectra of complex **Ru2** as a function of pH in the range 2–13 at 25 °C. Inset: A plot of absorbance against pH obtained at λ = 450 nm

A representative UV–Vis spectra obtained for **Ru2** is shown in Fig. 2. The inset displays an absorbance versus pH plot obtained at λ = 450 nm.

The acidity constants obtained were; 9.81 ± 0.03 (**Ru1**), 9.74 ± 0.02 (**Ru2**), 9.40 ± 0.03 (**Ru3**) and 8.78 ± 0.02 (**Ru4**). These values are comparable with those reported in the literature [13, 19]. It is notable that the acid constants of the complexes have a negative relationship with the π-conjugation of the auxiliary ligands; suggesting an upsurge in the π-acceptor ability of the ligands and electrophilicity indices of the complexes as the aromatic area of the auxiliary ligand is enlarged [22, 34].

As the π-acceptor ability of the auxiliary ligand increases the metal center becomes more depleted of negative charge due to enhanced withdrawal of electron cloud. Thus, making the aqua ligand more acidic [35]. At a pH of 1.0, all the aqua complexes exist exclusively as aqua species, hence an appropriate pH for the kinetic studies.

DFT-based computational results

Theoretical studies were performed to give more information on the structural and electronic properties of the studied aqua complexes. Geometry-optimized minimum energy structures of the complexes, mappings of the frontier orbitals of the complexes and planarity of the complexes are shown in Table 1. An extract of key computational data of the optimized complexes is collected in Table 2. Fig. 3 shows the typical atomic numbering in the complexes. All the complexes adopt distorted octahedral geometry in which Ru-N1 and Ru-N3 bond lengths are unequal, with the Ru-N2 bond being significantly shorter. This is attributable to the steric constraints imposed on N^N bidentate ligands by the meridionally anchored terpyridine ligand

Table 1 Geometry-optimized structures, mappings of frontier molecular orbitals and planarity for the studied complexes

Complex	HOMO	LUMO	Planarity
Ru1	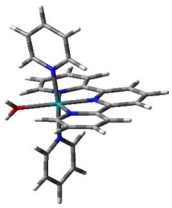	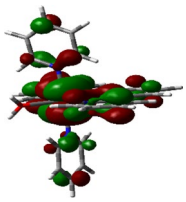	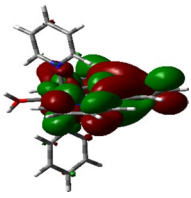	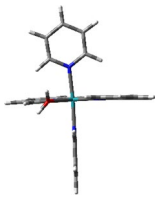
Ru2	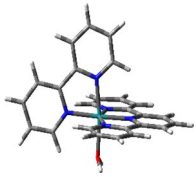	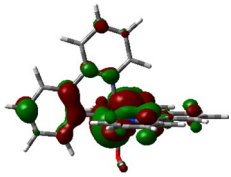	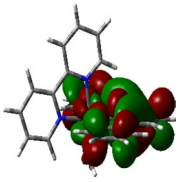	
Ru3	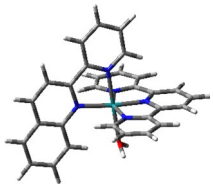	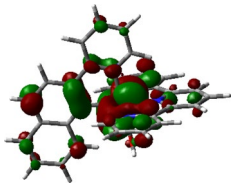	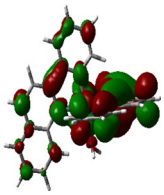	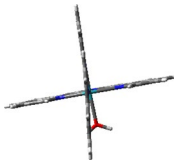
Ru4	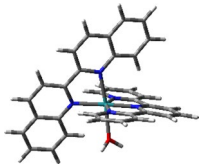	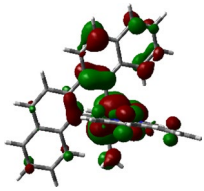	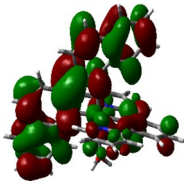	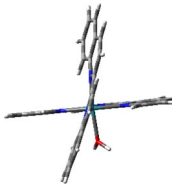

[10]. As a result, the angle N1-Ru-N3 deviates significantly from the expected 180° to range from 158.51° to 159.89°.

For complex **Ru1**, the two monodentate pyridyl auxiliary ligands are *trans* to each other and *cis* to the aqua labile ligand. For the rest of the complexes, the axially coordinated N-donor bidentate ligand (2,2′-bipyridyl, -2′(2-pyridyl)quinoline or 2,2′-biqunoline) have one of its rings *cis* while the other *trans* to the aqua ligand. The Ru-N4 bond lengths is longer than the Ru-N5's (Table 2), an indication of common asymmetrical coordination of the rings to the ruthenium metal centre due to the inter-ligand steric repulsions [36]. The angle N2-Ru-N5 was measured to determine the deviation of the optimized structures of the complexes from the optimal octahedral geometry. For the complexes, **Ru2–Ru4**, their bidentate ligands are tilted away from the terpyridine plane, making the N2-Ru-N5 angle greater than the expected 90°. The greatest deviation in the angle was observed in complex **Ru4**. The trend in this structural distortion is a manifestation of the increased steric repulsion between

Table 2 Extracted key computational data of the geometry-optimized structures of the studied complexes

Computational data/complex	**Ru1**	**Ru2**	**Ru3**	**Ru4**
Chemical descriptors				
HOMO (eV)	− 6.094	− 6.102	− 6.137	− 6.111
LUMO (eV)	− 2.845	− 2.862	− 2.943	− 3.147
$\Delta E_{HOMO\text{-}LUMO}$ (eV)	3.249	3.240	3.194	2.964
Chemical potential (eV)	− 4.470	− 4.482	− 4.453	− 4.629
Chemical hardness (eV)	1.625	1.620	1.597	1.482
Chemical softness (eV^{-1})	0.615	0.617	0.626	0.675
Electrophilicity Index (eV)	6.148	6.200	6.385	7.229
Atomic charge (Ru^{2+})	0.370	0.373	0.378	0.375
Dipole moment (D)	2.998	3.178	6.399	6.552
Bond length (Å)				
Ru-N1	2.106	2.104	2.103	2.100
Ru-N3	2.108	2.104	2.106	2.118
Ru-N2	1.964	2.001	1.997	2.006
Ru-N5		2.054	2.044	2.100
Ru-N4	2.130	2.090	2.168	2.123
Ru-OH_2	2.217	2.173	2.223	2.193
Bond angle/°				
N2-Ru-OH_2	179.27	89.84	83.26	81.19
N1-Ru-N3	159.89	158.53	158.81	158.51
N2-Ru-N5		98.50	96.23	103.36

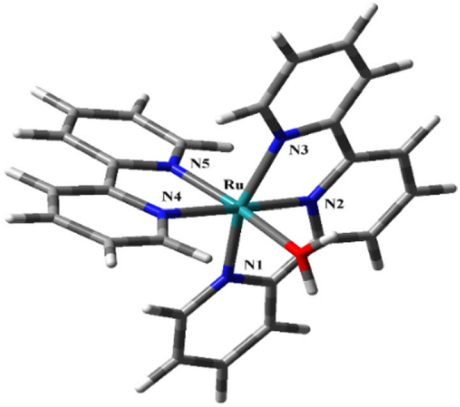

Fig. 3 Geometry-optimized molecular structure of complex **Ru2** showing typical labelling of the atoms in the complexes

the two chelating ligands as the size of the π-surface area of bidentate ligand increases incrementally from 2,2′-bipyridine to the 2,2′-biquinoline ligand [13].

From the optimized structures in Table 1, the electron density of the HOMO is largely based on Ru^{2+} ion for all the complexes. For **Ru1** and **Ru2**, the LUMO density is completely based on the terpyridine spectator ligand. On increasing the π-surface area of the auxiliary ligand from **Ru2** to **R4**, the LUMO density

increases proportionally to the number of rings on the ligand. Consequently, the LUMO density is higher on the more π-conjugated 2,2′-biquinoline ligand of **Ru4** in **Ru2** and **Ru3**. At the same time, its density on the terpyridine falls conversely. Accordingly, the stabilization of LUMO energy level of **Ru4** significantly lowers the energy bandgap by 0.2 eV compared to **Ru3**'s (Table 2).

The planarity of the coordinated terpyridine ligand remains unaffected by the change in the auxiliary ligand. However, as the π-surface of the auxiliary ligand is increased, the C–C bridged rings of the bidentates are inclined non-linearly about the bond and on the side that is away from the terpyridine's plane. The distortion in planarity of the bidentate ligand occurs more for the 2,2′-biquinoline. This is shown by the larger dihedral angle between the two quinolinyl moiety planes of 14.79° in **Ru4** compared to 5.26° between the pyridyl and quinolinyl and planes in **Ru3** (Fig. ESI 1 and 2, Electronic Supplementary Information). In complex **Ru2**, no significant distortion was observed for the bidentate ligand.

Kinetics results

The substitution reactions of the four complexes using three thiourea nucleophiles was monitored by observing the change in UV–Vis absorbance at a chosen wavelength over time. Fig. 4 shows a representative spectra observed for the reaction of **Ru1** with 1,1-dimethylthiourea.

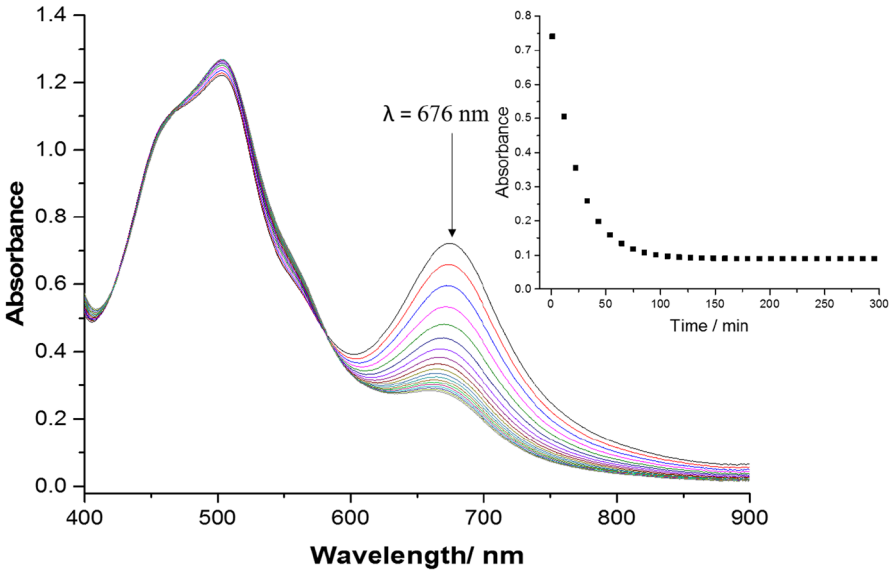

Fig. 4 UV–Vis spectra for the reaction of complex **Ru1** (0.421 mM) with 1,1-dimethylthiourea (0.421 M) at 25 °C, pH = 1.0, Ionic strength = 0.1 M $HClO_4/NaClO_4$. Inset: Absorbance-time trace obtained for reaction of complex **Ru1** with 1,1-dimethylthiourea at λ = 676 nm

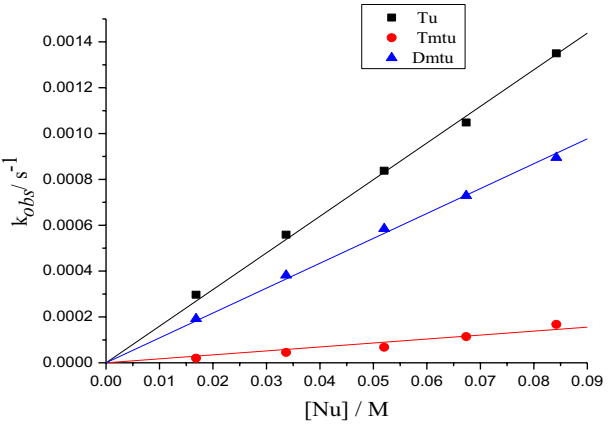

Fig. 5 Plots of observed rate constants versus concentration for the substitution of the aqua ligand from **Ru1** by thiourea nuclephiles. Key: Tu -thiourea, Dmtu -1,1-dimethylthiourea, Tmtu-1,1,3,3-tetramethylthiourea

Table 3 Summary of k_2, $\Delta H^{\neq}$ and $\Delta S^{\neq}$ for the substitution reactions of the complexes

Complex	Nucleophile	k_2 (10^{-2} M^{-1} s^{-1}) (298.15 K)	$\Delta H^{\neq}$ (kJ mol^{-1})	$\Delta S^{\neq}$ (J mol^{-1} K^{-1})
Ru1	Thiourea	1.60 ± 0.02	46 ± 1	− 126 ± 3
	1,1-dimethylthiourea	1.09 ± 0.01	54 ± 2	− 102 ± 6
	1,1,3,3-tetramethylthiourea	0.17 ± 0.01	60 ± 1	− 98 ± 3
Ru2	Thiourea	0.06 ± 0.01	72 ± 2	− 63 ± 8
	1,1-dimethylthiourea	0.12 ± 0.01	69 ± 2	− 71 ± 8
	1,1,3,3-tetramethylthiourea	0.05 ± 0.01	84 ± 2	− 26 ± 8
Ru3	Thiourea	13.85 ± 0.30	37 ± 1	− 137 ± 3
	1,1-dimethylthiourea	7.65 ± 0.20	49 ± 3	− 101 ± 8
	1,1,3,3-tetramethylthiourea	0.34 ± 0.03	66 ± 2	− 72 ± 8
Ru4	Thiourea	21.97 ± 0.40	42 ± 2	− 117 ± 7
	1,1-dimethylthiourea	35.03 ± 0.30	40 ± 2	− 119 ± 7
	1,1,3,3-tetramethylthiourea	3.67 ± 0.20	57 ± 2	− 79 ± 5

Pseudo-first order rate constants (k_{obs}) for the reactions were obtained by fitting the kinetic traces taken at the suitable wavelength onto the standard single-exponential decay function [37]

The k_{obs} values are for all reaction are found in Tables S1–S4. A positive linear relationship between k_{obs} values and nucleophile concentration was oserved in all the complexes. In addition, no indication of the reverse or solvolytic reaction was observed, since all the the plots of k_{obs} versus nucleophile recorded a zero y-intercept. A typical plots of k_{obs} against concentration are shown in Fig. 5. The second-order rate constant (k_2) were obtained from the plots of k_{obs} against nuclephile concentrations. The k_2 values obtained for the complexes are found in Table 3.

All these concentration-dependent substitution reaction obeyed the rate law given in Eq. (2).

$$k_{obs} = k_2[\text{Nucleophile}] \tag{2}$$

To determine the thermodynamic parameters of the substitution process, the reaction temperature was varied systematically from 298 to 318 at an interval of 5 K. The activation enthalpy ($\Delta H^{\neq}$) and entropy ($\Delta S^{\neq}$) were then calculated using the Eyring Eq. (3) [37].

$$ln\left(\frac{k_2}{T}\right) = \left(-\frac{\Delta H^{\neq}}{R}\right)\frac{1}{T} + \left(23.78 + \frac{\Delta S^{\neq}}{R}\right) \tag{3}$$

Representative Eyring plots obtained for the complexes are shown in Fig. 6 and the values of activation enthalpy and entropy for the complexes are presented in Table 3. The k_{obs} obtained at different temperatures and constant nucleophilic concentrations are presented in Tables S5a, S6a, S7a and S8a. $ln\left(\frac{k_2}{T}\right)$ and their respective $\frac{1}{T}$ values are collected in the Electronic Supplementary Information (Tables S5b, S6b, S7b and S8b).

Product analysis: crystal structure of bipyridineterpyridinethiourearuthenium(II) perchlorate

The data obtained from x-ray crystallographic analysis show important information about the complex. Ellipsoidal molecular structure of the complex is shown in

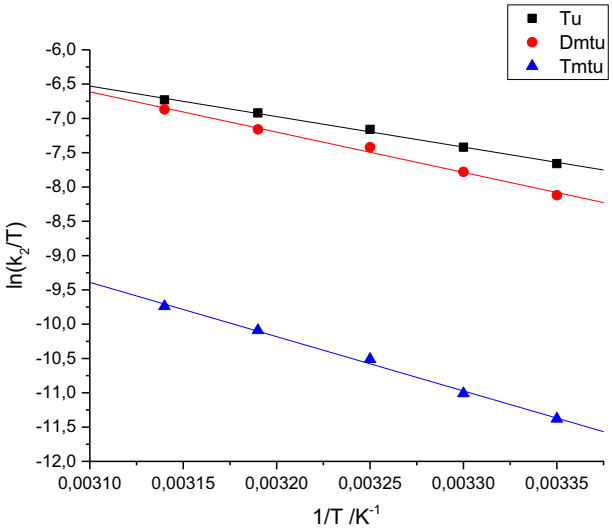

Fig. 6 Eyring plots obtained for the substitution reaction of complex **Ru3**. Key: Tu -thiourea, Dmtu -1,1-dimethylthiourea, Tmtu-1,1,3,3-tetramethylthiourea

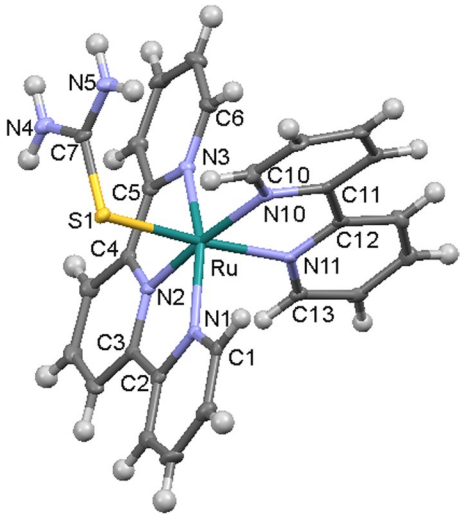

Fig. 7 Ellipsoidal molecular structure of bipyridineterpyridin ethiourearuthenium(II) perchlorate plotted at 50% probability (counterions omitted for clarity)

Table 4 Crystallographic data and structure refinement parameters

Parameters	Data
Empirical formula	$C_{26}H_{23}Cl_2N_7O_8SRu$
Formula weight/gmol^{-1}	765.54
Crystal system	Monoclinic
Space group	P 21/c
a/Å	9.28(15)
b/Å	26.21(4)
c/Å	11.93(2)
α/°	90
β/°	99.21(4)
γ/°	90
Volume/Å^3	2864.5(8)
Z	4
Density (Calc)/g cm^{-3}	1.775
Absorption coefficient/mm^{-1}	0.871
F(000)	1544
Crystal size/mm^3	0.56×0.160×0.140
Goodness-of-fit on F^2/%	99.3
Index ranges	$-11 \le h \le 11$, $-34 \le k \le 33, -15 \le l \le 15$
Final R indices [I > 2σ(I)]	$R1 = 0.0543$, $wR_2 = 0.1181$
R indices (all data)	$R1 = 0.0711$, $wR_2 = 0.1274$

Fig. 7 while selected crystallographic and structure refinement parameters are presented in Table 4. Important interatomic distances and angles of the crystal structure and geometry-optimized structure of the complex are collected in Table 5. More

Table 5 Key bond lengths and bond angles for bipyridineterpyridinethiourearuthenium(II) perchlorate complex

Bond length (Å)		
Bond crystal		DFT
Ru-S1	2.430 (11)	2.476
Ru-N1	2.066 (4)	2.113
Ru-N2	1.965 (3)	1.997
Ru-N3	2.088 (3)	2.105
Ru-N10	2.087 (3)	2.112
Ru-N11	2.074 (3)	2.073
Bond angle (°)		
Bond angle crystal		DFT
N2-Ru-N1	79.89 (14)	79.20
N2-Ru-N3	79.42 (14)	79.38
N1-Ru-N3	159.31 (13	158.29
N2-Ru-S1	90.69 (10)	88.57
N3-Ru-S1	94.74 (9)	92.99
N1-Ru-S1	85.31 (9)	87.05
N10-Ru-S1	95.92 (9)	96.18
N11-Ru-S1	173.89 (9)	171.79

information about the crystal structures at be accessed at CCDC refcode, NIGHOD [38].

The complex has two ClO_4^- counterions, showing that the 2+ oxidation state of the ruthenium metal centre is maintained after the reaction with thiourea. The complex adopts slightly distorted octahedral geometry in which all the Ru-N(terpyridine) bond lengths are typical of ruthenium terpyridine complexes [10, 19, 39–41]. The Ru-N2 bond is slightly shorter than the Ru-N1 and Ru-N3 bonds. This behaviour has been reported in other complexes and is attributable to geometric and steric constraints imposed on the tridentate terpyridine ligand on coordination to the metal centre. As a result, the terpyridine's bite angle deviates from the expected 180° to 159.31° [41].

The terpyridine ligand is slightly twisted as shown by an average tilt angle of 2.71° between the central and terminal pyridyl rings. The thiourea ligand is coordinated to the metal centre via the S-donor atom with the Ru-S bond length within the reported range (2.304–2.427 Å) [42–44]. The bipyridyl ligand is asymmetrically coordinated to the metal centre with the Ru-N bond *cis* to the thiourea (Ru-N10) slightly longer than the *trans* one (Ru-N11). The difference in length is attributed to inter-ligand steric repulsions [36]. The two pyridyl rings of the bipyridyl ligand are non-planar, with a dihedral angle of 11.89° between them.

The planes RuN1N2N3N10 and RuS1N2N10N11 are near orthogonal to each other with a dihedral angle of 84.93°. This distortion from expected octahedral geometry is attributed to constraints caused by the bite angles of the bipyridyl and

terpyridine spectator ligands. The crystal packing of the complex is dominated by van der Waals forces. The crystal's bond lengths and angles compare well with those obtained from DFT-optimized minimum structure of the complex. Thus, benchmarking favourably the DFT theoretical calculations as applied in the aqua complexes.

Discussion

The k_2 values obtained for the substitution of the labile aqua ligand from the four ruthenium(II) complexes by thiourea will be used as a representative to discuss the reactivity of the complexes. The variance in the substitution reactivity of the complexes, are due to inherent electronic and steric properties of the axial auxiliary spectator ligand since the terpyridine ligand anchors the equatorial plane for all the complexes. In complex **Ru1**, the auxiliary groups are two moderate π-acceptor and weak σ-donor *trans*-coordinated pyridyl rings [45]. For the rest of the complexes, the auxiliary spectator ligand is an axially coordinated-bidentate ligand (2,2′-bipyridyl, 2′-(2-pyridyl)quinoline or 2,2′-biquinoline) in which the labile aqua ligand lies in the same plane as the bidentate ligand. Thus, the latter exerts an in-plane steric effect on the aqua ligand [46]. The steric bulkiness and the π-surface area of the auxiliary ligand increase incrementally from complex **Ru2** to **Ru4**.

On the basis of the π-suface area of the complexes, the trend in the substitution reactivity is expected to be; **Ru1** < **Ru2** < **Ru3** < **Ru4**. This is because the π-acceptor properties of the auxiliary ligand gradually increase from the 2,2′-bipyridyl ligand in **Ru2** to **Ru4** by successive extensions of the π-conjugation of the bidentate ligands [22, 45, 47–49]. Conversely, complex **Ru1** was found to be about 27 times more reactive than **Ru2**. The depressed reactivity in **Ru2** is due to the 2,2′-bipyridyl bidentate auxiliary ligand which offers more steric hindrance to the incoming group than the two independent pyridyl auxiliary ligands in **Ru1**. The increased steric hindrance in complex **Ru2** slows the formation rate of the transition state by impeding the facile attack of the ruthenium metal centre by the incoming group. The Ru-OH_2 bond is markedly shorter in **Ru2** (2.17 Å) compared to **Ru1** (2.22 Å). As a result, the labile aqua ligand in **Ru2** is more strongly held than the aqua ligand in **Ru1**. This makes its displacement harder and leads to a lower rate constant as experimentally observed [10, 39].

As observed from the frontier molecular orbitals mappings (Table 1), the contribution of the coordinated auxiliary ligand to the LUMO is positively correlated to the π-conjugation of the ligands. Extending the π-conjugation of the auxiliary ligand leads to sequential stabilization of this molecular orbital as revealed by the decreasing trend of their energies [22, 50]. Consequently, the energy gap between the HOMO and LUMO reduces and the interaction between the two orbitals rises as one moves from **Ru1** to **Ru4**. The electron affinity of the complexes is thus increased in the same order as it becomes easier for π-back bonding to take place. As a result, the rate of displacement of the labile aqua ligand is enhanced as the π-conjugation of the auxiliary ligand is increased.

Additionally, as the π-conjugation of the auxiliary ligand increases, the stabilization of the entering electron density becomes more effective since density is spread over a larger π-surface area [22]. Thus, an increase in aromatic area of the auxiliary ligand is positively correlated with increase in the chemical softness of the complexes as shown in Table 2. Further corroboration of the reactivity trends is provided by the trend in the global electrophilicity index of the complexes, a parameter which is calculated from the electronic chemical potentials and the chemical hardness [51, 52]. The former is a superior parameter for describing the tendency of a complex to accept electrons because it measures its ability to gain an extra electronic charge and its resistance to exchange the gained electronic charge with its immediate environment [53]. Therefore, it describes holistically the charge distribution within the entire complex better than other quantum descriptors [31]. The computationally obtained global electrophilicity indices show a positive correlation with the observed reactivity trend except for complex **Ru1**, whose anomalous substitution reactivity has been discussed (vide supra). The calculated data predict **Ru4** to be the strongest electrophile and thus the most reactive [51].

We noted that complex **Ru4** is only slightly more reactive than complex **Ru3**, inspite of its bigger aromatic surface area and higher electrophilicity. This is explained by the increased steric hindrance to the the incoming nucleophile brought about by the large and bulky 2,2′-biquinoline bidentate auxiliary ligand therein. From the minimum energy DFT-optimized molecular structure of **Ru4,** the 2,2′-biquinoline ligand adopts an out-of plane banana shaped curvature conformation (Table 1). The steric interaction between the 2,2′-biquinoline auxiliary ligand and the terpyridine principal ligand is increased by the large in-plane size of the former [54, 55] as shown by the larger N2-Ru-N5 angle in **Ru4** (103.4°) compared to **Ru3** (96.2°). Accordingly, the access of metal centre by the incoming group becomes more restricted. From the minimum energy structures, it was noted that the dihedral angle between the two planes of the quinolinyl groups in **Ru4** is 14.79° compared to 5.26° between the planes of quinolinyl and pyridyl moieties in **Ru3** (Electronic Supplementary Information, Fig. SI 1–2). This significant distortion of planarity of the 2,2′-biquinoline bidentate ligand lowers its π-back-donation ability, leading to a less positive metal centre [54, 56] as shown by the slightly lower ruthenium atomic charge in **Ru4**. The lower charge of ruthenium metal centre in **Ru4** is also attributable to the σ-donicity of the 2,2′-biquinoline ligand since it is endowed with both π-acceptor and σ-donor properties [56]. Largely, the effect of this is decreased substitution reactivity.

Absorption electronic transitions and redox potentials have been used to determine the extend of electrophilicity of coordination and organometallic compounds. For instance; when the auxiliary ligand is varied from 2,2′-bipyridine to 2,2′-biquinoline, the initial reduction potential increase because the energy of π* orbital is more stabilized [12, 57–59]. The changes in reduction potential corroborate the fact that the π-acceptor abilities of the subsidiar ligand rise with increase in π-conjugation of the ligands. Likewise, the distinctive metal to ligand charge transfer absorption band undergoes bathochromic shift when the auxiliary ligand is varied from 2,2′-bipyridine to 2,2′-biquinoline [19, 59]. This agrees with the reduction in energy gap

between frontier orbitals as π-surface area of the spectator ligand increases. Therefore, the ability of the auxiliary ligands to withdraw electron density from the metal centre is expected to increase from 2,2′-bipyridine to 2,2′-biquinoline.This supports the observed increasing trend in electrophilicity indices as one moves from **Ru2** to **Ru4**.

A negative relationship was observed between the pKa values of the complexes and the π-conjugation of the auxiliary ligands in the complexes. This implies that the acidity of the labile aqua ligands increases from **Ru1** to **Ru4**. This trend can be attributed to an increase in the π-acceptor ability of the ligands as one moves from **Ru1** to **Ru4** which enhances the withdrawal of electron density from the metal centre in that order [25, 35]. This is supported by the increase in the dipole moments from **Ru1** to **Ru4** [60]. The trend in the pKa values and DFT-calculated electrophilicity indices affirms that when π-conjugation of the bidentate auxilliary ligand increases, the electrophilicity of the complexes rise causing the observed increase in substitution reactivity from **Ru2** to **Ru4**.

Theoretically, the trends in substitution reactivity with respect to the nucleophiles is expected to be; Thiourea > 1,1-dimethylthiourea > 1,1,3,3-tetramethylthiourea in order of increasing steric bulkiness. However, from the results obtained it was found that, in complexes **Ru2** and **Ru4**, the more sterically demanding 1,1-dimethylthiourea reacted faster than the unhindered thiourea. This is due to the inductive effect caused by the two methyl groups in 1,1-dimethylthiourea leading to overcompensation of the steric effect [22].

The negative activation entropy values observed for all the complexes show that the reactions follow an associative interchange mechanism. Since all the reactions were carried out in aqua media, the precursor formation was weak and therefore no non-linearity was observed in the plots of k_{obs} versus nucleophilic concentrations. These values imply that the transition state is more ordered than the starting reagents. Associative interchange substitution mechanism has also been observed in other ruthenium(II) complexes [6, 9, 11, 39].

Conclusion

It has been established that the substitution reactivity of ruthenium(II) aqua complexes with common terpyridine ligand and N (pyridine) or N^N (2,2′-bipyridyl, 2′-(2-pyridyl)quinoline or 2,2′-biqunoline) auxiliary ligand(s) are strongly dependent on the steric and electronic characteristics of the coordinated auxiliary ligands. From **Ru2** to **Ru4,** the substitution reactivity depends on the π-acceptor ability of the bidentate auxiliary ligand which is positively correlated with the aromatic surface area. As the aromatic surface area is extended, the ruthenium(II) complexes become more electrophilic and hence more reactive. It was found that complex **Ru1** is more reactive than **Ru2**. This is because the 2,2-bipyridyl bidentate auxiliary ligand in **Ru2** offers more steric hindrance to the incoming group than the two *trans* pyridyl monodentate rings in **Ru1**. Trends in the theoretically calculated quantum descriptors indicate a systematic stabilization of the LUMO energy and narrowing of the energy gap between the HOMO and LUMO as the

π-conjugation of the auxiliary ligand is extended from **Ru1** to **Ru4** leading to increased electrophilicity indices of the complexes. Similarly, the pKa values of the complexes reduce as one moves from **Ru1** to **Ru4** inferring that the acidity of the labile aqua ligand increases from **Ru1** to **Ru4**. Thus, trends in both the theoretical calculations and acidity constants support the observed trend in reactivity except in **Ru1**. The reactions in the four complexes follow an associative mechanism. The solid state crystal structure of bipyridineterpyridinethiourearuthenium (II) perchlorate show that terpyridine ruthenium(II) thiourea complexes are stable and the thiourea is coordinated to the metal centre via the S-donor atom.

Supplementary Information The online version contains supplementary material available at https://doi.org/10.1007/s11144-022-02272-0.

Acknowledgements We authors acknowledge Masinde Muliro University of Science and Technology, Kenya for its financial support. We thank Mr. Craig Grimmer and Ms. Caryl Janse van Rensburg for their assistance in characterization of the complexes.

Funding This research was funded by the University of KwaZulu-Natal, South Africa.

Declarations

Conflict of interest No potential conflict of interest was reported by the authors.

References

1. Udvardy A, Joó F, Kathó Á (2021) Synthesis and catalytic applications of Ru(II)-phosphaurotropine complexes with the use of simple water-soluble Ru(II)-precursors. Coord Chem Rev 438:213871. https://doi.org/10.1016/j.ccr.2021.213871
2. Lin K, Zhao Z-Z, Bo H-B et al (2018) Applications of ruthenium complex in tumor diagnosis and therapy. Front Pharmacol. https://doi.org/10.3389/fphar.2018.01323
3. Winter A, Schubert US (2020) Metal-terpyridine complexes in catalytic application–a spotlight on the last decade. ChemCatChem 12:2890–2941. https://doi.org/10.1002/cctc.201902290
4. Savic M, Arsenijevic A, Milovanovic J et al (2020) Antitumor activity of ruthenium (II) terpyridine complexes towards colon cancer cells in vitro and in vivo. Molecules 25:4699. https://doi.org/10.3390/molecules25204699
5. Paul S, Kundu P, Kondaiah P, Chakravarty AR (2021) BODIPY-ruthenium(II) bis-terpyridine complexes for cellular imaging and type-I/-II photodynamic therapy. Inorg Chem 60:16178. https://doi.org/10.1021/acs.inorgchem.1c01850
6. Sitati MK, Mutua GK, Onunga DO et al (2021) The effect of substituents on the reactivity of dichloridotriphenylphosphinoruthenium (II) complexes: kinetic and mechanistic study. J Coord Chem 74:1349. https://doi.org/10.1080/00958972.2021.1904234
7. Mambanda A, Jaganyi D (2017) Controlling the lability of square-planar Pt (II) complexes through electronic and π-conjugation: correlation between kinetics and theoretical parameters. Advances in inorganic chemistry. Elsevier, Amsterdam, pp 243–276. https://doi.org/10.1016/bs.adioch.2017.03.001
8. Ongoma P, Jaganyi D (2012) The π-acceptor effect in the substitution reactions of tridentate N-donor ligand complexes of platinum (ii): a detailed kinetic and mechanistic study. Dalton Trans 41:10724. https://doi.org/10.1039/C2DT31041D
9. Ćoćić D, Chrzanowska M, Katafias A et al (2021) Tuning the lability of a series of Ru(II) polypyridyl complexes: a comparison of experimental-kinetic and DFT-predicted reaction mechanisms. J Coord Chem 74:433. https://doi.org/10.1080/00958972.2021.1874369

10. Milutinović MM, Elmroth SK, Davidović G et al (2017) Kinetic and mechanistic study on the reactions of ruthenium (II) chlorophenyl terpyridine complexes with nucleobases, oligonucleotides and DNA. Dalton Trans 46:2360. https://doi.org/10.1039/C6DT04254F
11. Chrzanowska M, Katafias A, Kozakiewicz A, van Eldik R (2020) Steric and electronic tuning of the reactivity of [Ru^{II}(terpy)(N^N)Cl]Cl complexes. Inorg Chim Acta 504:119449. https://doi.org/10.1016/j.ica.2020.119449
12. Bessel CA, Margarucci JA, Acquaye JH et al (1993) Steric ligand effects of six bidentate bipyridyl ligands. Inorg Chem 32:5779. https://doi.org/10.1021/ic00077a021
13. Tiba F, Jaganyi D, Mambanda A (2010) Meridional anchorage of coordinate occupancy by a planar tridentate ligand and its effect on ligand substitution reactions of octahedral ruthenium (II) complexes. J Coord Chem 63:2542. https://doi.org/10.1080/00958972.2010.507269
14. Schiessl WC, Summa NK, Weber CF et al (2005) Experimental and theoretical approaches to the protonation of thiourea: a convenient nucleophile in coordination chemistry revisited. Z Für Anorg Allg Chem 631:2812. https://doi.org/10.1002/zaac.200500157
15. Zhao Q, Liu S, Shi M et al (2006) Series of new cationic iridium (III) complexes with tunable emission wavelength and excited state properties: structures, theoretical calculations, and photophysical and electrochemical properties. Inorg Chem 45:6152. https://doi.org/10.1021/ic052034j
16. Sullivan BP, Calvert JM, Meyer TJ (1980) Cis-trans isomerism in (trpy)(PPh_3) $RuC1_2$. Comparisons between the chemical and physical properties of a cis-trans isomeric pair. Inorg Chem 19:1404. https://doi.org/10.1021/ic50207a066
17. Suen HF, Wilson S, Pomerantz M, Walsh JL (1989) Photosubstitution reactions of terpyridine complexes of ruthenium (II). Inorg Chem 28:786. https://doi.org/10.1021/ic00303a034
18. Takeuchi KJ, Thompson MS, Pipes DW, Meyer TJ (1984) Redox and spectral properties of monooxo polypyridyl complexes of ruthenium and osmium in aqueous media. Inorg Chem 23:1845. https://doi.org/10.1021/ic00181a014
19. Hirahara M, Hakamata T, League AB et al (2015) Mechanisms and factors controlling photoisomerization equilibria, ligand exchange, and water oxidation catalysis capabilities of mononuclear ruthenium(II) complexes. Eur J Inorg Chem 2015:3892. https://doi.org/10.1002/ejic.201500642
20. OriginPro9.1, OriginLab Corporation, One Roundhouse Plaza, Suite 303, Northampton, MA 01060, United States, 2014 1800-969-7720. www.OriginLab.com
21. Bugarčić ŽD, Petrović BV, Jelić R (2001) Hydrolysis of [Pt (dien)H_2O]$^{2+}$ and [Pd(dien)H_2O]$^{2+}$ complexes in water. Transit Met Chem 26:668. https://doi.org/10.1023/A:1012064512961
22. Hofmann A, Dahlenburg L, van Eldik R (2003) Cyclometalated analogues of platinum terpyridine complexes: kinetic study of the strong σ-donor cis and trans effects of carbon in the presence of a π-acceptor ligand backbone. Inorg Chem 42:6528. https://doi.org/10.1021/ic034400+
23. Frisc M, Trucks G, Schlegel H, Scuseria G, Robb M, Cheeseman J, Scalmani G, Barone V, Mennucci B, Petersson G et al (2009) Gaussian 09 (Revision C.01). Gaussian Inc, Wallingford CT. http://www.Gaussian.com
24. Li J, Xu L-C, Chen J-C et al (2006) Density functional theory/time-dependent DFT studies on the structures, trend in DNA-binding affinities, and spectral properties of complexes [Ru(bpy)$_2$(p-R-pip)] $^{2+}$(R=−OH,−CH_3,−H,−NO_2). J Phys Chem A 110:8174. https://doi.org/10.1021/jp0564389
25. Gupta V (2015) Principles and applications of quantum chemistry. Elsevier Inc., London, pp 156–175. https://doi.org/10.1016/C2014-0-05143-X
26. Okamura M, Yoshida M, Kuga R et al (2012) A mononuclear ruthenium complex showing multiple proton-coupled electron transfer toward multi-electron transfer reactions. Dalton Trans 41:13081. https://doi.org/10.1039/C2DT30773A
27. Cossi M, Scalmani G, Rega N, Barone V (2002) New developments in the polarizable continuum model for quantum mechanical and classical calculations on molecules in solution. J Chem Phys 117:43. https://doi.org/10.1063/1.1480445
28. Parr RG, Szentpaly LV, Liu S (1999) Electrophilicity index. J Am Chem Soc 121:1922. https://doi.org/10.1021/ja983494x
29. Pearson RG (1992) The electronic chemical potential and chemical hardness. J Mol Struct Theochem 255:261. https://doi.org/10.1016/0166-1280(92)85014-C
30. Pearson RG (1992) Chemical hardness and the electronic chemical potential. Inorg Chim Acta 198:781. https://doi.org/10.1016/S0020-1693(00)92423-X
31. Wekesa IM, Jaganyi D (2014) Kinetic and mechanistic studies of 1,3-bis (2-pyridylimino) isoindolate Pt (II) derivatives. Experimental and new computational approach. Dalton Trans 43:2549. https://doi.org/10.1039/C3DT52272E

32. Dolomanov OV, Bourhis LJ, Gildea RJ et al (2009) OLEX2: a complete structure solution, refinement and analysis program. J Appl Crystallogr 42:339. https://doi.org/10.1107/S0021889808042726
33. Sheldrick GM (2015) Crystal structure refinement with SHELXL. Acta Crystallogr C 71:3. https://doi.org/10.1107/S2053229614024218
34. Peacock AF, Habtemariam A, Moggach SA et al (2007) Chloro half-sandwich osmium (II) complexes: influence of chelated N, N-ligands on hydrolysis, guanine binding, and cytotoxicity. Inorg Chem 46:4049. https://doi.org/10.1021/ic062350d
35. Pizarro AM, Habtemariam A, Sadler PJ (2010) Activation mechanisms for organometallic anticancer complexes. In: Medicinal organometallic chemistry. Springer, Berlin, pp 21–56. https://doi.org/10.1007/978-3-642-13185-1-2
36. Hecker CR, Fanwick PE, McMillin DR (1991) Evidence for dissociative photosubstitution reactions of (acetonitrile)(bipyridine)(terpyridine)ruthenium(2+). Crystal and molecular structure of [Ru(trpy)(bpy)(py)]$(PF_6)_2$.cntdot. $(CH_3)_2CO$. Inorg Chem 30:659–666. https://doi.org/10.1021/ic00004a013
37. Atwood JD (1997) Inorganic and organometallic reaction mechanisms, 2nd edn. VCH Publishers, New York, pp 1–18, 47–90
38. Mutua GK, Jaganyi D (2018) CCDC 1811063: experimental crystal structure determination. https://doi.org/10.5517/ccdc.csd.cc1yskdp. https://www.ccdc.cam.ac.uk/mystructures/structuredetails/0758cbc9-1be0-e711-8534-005056868fc8.
39. Chrzanowska M, Katafias A, Impert O et al (2017) Structure and reactivity of $[Ru^{II}$(terpy)(N^N)Cl]Cl complexes: consequences for biological applications. Dalton Trans 46:10264. https://doi.org/10.1039/C7DT01669G
40. Huang H, Zhang P, Chen Y et al (2016) Synthesis, characterization and biological evaluation of labile intercalative ruthenium(II) complexes for anticancer drug screening. Dalton Trans 45:13135. https://doi.org/10.1039/C6DT01270A
41. Walsh JL, McCracken R, McPhail AT (1998) Preparation and X-ray crystal structure study of a polypyridyl ruthenium (II) complex containing a dehydrodithizone ligand. Polyhedron 17:3221. https://doi.org/10.1016/S0277-5387(98)00095-3
42. Vijayan P, Viswanathamurthi P, Sugumar P et al (2017) Solvent-assisted formation of ruthenium (II)/Copper (I) complexes containing thiourea derivatives: synthesis, crystal structure, density functional theory, enzyme mimetics and in vitro biological perspectives. Appl Organomet Chem 31:1. https://doi.org/10.1002/aoc.3652
43. Douglas G, Muir KW, Patel A, Richens D (1991) Synthesis and structure of *hexakis* (thiourea) ruthenium (II) trifluoromethanesulfonate. Acta Crystallogr C 47:1394. https://doi.org/10.1107/S0108270191000793
44. Fairlie DP, Wickramasinghe WA, Byriel KA, Taube H (1997) Activation of thiourea bound through sulfur to pentaammineruthenium (III): structure and reactivity. Inorg Chem 36:2242. https://doi.org/10.1021/ic9611397
45. Dougan SJ, Melchart M, Habtemariam A et al (2006) Phenylazo-pyridine and phenylazo-pyrazole chlorido ruthenium(II) arene complexes: arene loss, aquation, and cancer cell cytotoxicity. Inorg Chem 45:10882. https://doi.org/10.1021/ic061460h
46. Huynh MHV, Smyth J, Wetzler M et al (2001) Remarkable rate enhancement of ligand substitution promoted by geometrical arrangement of tridentate "spectator" ligands. Angew Chem 113:4601. https://doi.org/10.1002/1521-3773(20011203)40:23%3c4469::AID-ANIE4469%3e3.0.CO;2-3
47. Jaganyi D, Hofmann A, van Eldik R (2001) Controlling the lability of square-planar PtII complexes through electronic communication between π-acceptor ligands. Angew Chem Int Ed 40:1680. https://doi.org/10.1002/1521-3773(20010504)40:9%3c1680::AID-ANIE16800%3e3.0.CO;2-K
48. Hu Y-Z, Zhang G, Thummel RP (2003) Friedländer approach for the incorporation of 6-bromoquinoline into novel chelating ligands. Org Lett 5:2251. https://doi.org/10.1021/ol034559q
49. Reddy D, Jaganyi D (2006) Does increased chelation enhance the rate of ligand substitution at Pt II (N, N, N) centres? A detailed kinetic & mechanistic study. Transit Met Chem 31:792. https://doi.org/10.1007/s11243-006-0071-8
50. Hanson K, Roskop L, Djurovich PI et al (2010) A paradigm for blue-or red-shifted absorption of small molecules depending on the site of π-extension. J Am Chem Soc 132:16247. https://doi.org/10.1021/ja1075162
51. Mebi CA (2011) DFT study on structure, electronic properties, and reactivity of *cis*-isomers of $[(NC_5H_4\text{-}S)_2Fe(CO)_2]$. J Chem Sci 123:727. https://doi.org/10.1007/s12039-011-0131-2

52. Chattaraj PK, Roy DR (2007) Update 1 of: electrophilicity index. Chem Rev 107:RR46. https://doi.org/10.1021/cr078014b
53. Ben El Ayouchia H, Anane H, El Idrissi Moubtassim ML et al (2016) A theoretical study of the relationship between the electrophilicity ω index and hammett constant σp in [3+2] cycloaddition reactions of Aryl Azide/alkyne derivatives. Molecules 21:1434. https://doi.org/10.3390/molecules21111434
54. Spek A, Gerli A, Reedijk J (1994) (2,2'-Biquinoline-κ2N, N') chloro (2,2': 6', 2''-terpyridine-κ^3N, N', N'') ruthenium (II) hexafluorophosphate,[$RuCl_{(C}1_{8H}1_2N2)_{(C}1_{5H}1_1N3)$][$_P$F6]. Acta Crystallogr C 50:394. https://doi.org/10.1107/S0108270193010236
55. Johnson BA, Agarwala H, White TA et al (2016) Judicious ligand design in ruthenium polypyridyl CO_2 reduction catalysts to enhance reactivity by steric and electronic effects. Chem- Eur J 22:14870. https://doi.org/10.1002/chem.201601612
56. Knoll JD, Albani BA, Durr CB, Turro C (2014) Unusually efficient pyridine photodissociation from Ru (II) complexes with sterically bulky bidentate ancillary ligands. J Phys Chem A 118:10603. https://doi.org/10.1021/jp5057732
57. Yoshikawa N, Sakamoto J, Matsumura-Inoue T et al (2004) Electrochemical and phosphorescent properties of new Ir (III) complexes coordinated by various bipyridine derivatives. Anal Sci 20:711. https://doi.org/10.2116/analsci.20.711
58. Heijden M, Van Vliet PM, Haasnoot JG, Reedijk J (1993) Synthesis and characterization of cis-(2,2′-bipyridine)(2,2′-biquinoline) dichlororuthenium (II) and its co-ordination chemistry with imidazole derivatives. J Chem Soc Dalton Trans. https://doi.org/10.1039/DT9930003675
59. Tseng H-W, Zong R, Muckerman JT, Thummel R (2008) Mononuclear ruthenium (II) complexes that catalyze water oxidation. Inorg Chem 47:11763. https://doi.org/10.1021/ic8014817
60. Rillema DP, Cruz AJ, Moore C et al (2012) Electronic and photophysical properties of platinum (II) biphenyl complexes containing 2,2′-bipyridine and 1,10-phenanthroline ligands. Inorg Chem 52:596. https://doi.org/10.1039/C5DT01891A

Authors and Affiliations

Gershom Kyalo Mutua[1,2] · Meshack Sitati[1,3] · Daniel O. Onunga[1,4] · Deogratius Jaganyi[5,6] · Allen Mambanda[1]

1 School of Chemistry and Physics, University of KwaZulu-Natal, Private Bag X01, Scottsville, Pietermaritzburg 3209, South Africa

2 Department of Pure and Applied Chemistry, Masinde Muliro University of Science and Technology, P.O Box 190-50100, Kakamega, Kenya

3 Department of Mathematics and Physical Sciences, Maasai Mara University, P.O Box 861, Narok 20500, Kenya

4 Department of Chemistry, Maseno University, P.O. Box 333-40105, Maseno, Kenya

5 School of Pure and Applied Sciences, Mount Kenya University, P.O. Box 342-01000, Thika, Kenya

6 Department of Chemistry, Faculty of Applied Sciences, Durban University of Technology, P.O Box 1334, Durban 4000, South Africa